Int. J. Multiphase Flow Vol. 11, No. 2, pp. 177–188, 1985
Printed in the U.S.A.

0301-9322/85 $3.00 + .00
Pergamon/Elsevier

PIPE FLOW WITH SOLID PARTICLES FIXED IN SPACE

YUTAKA TSUJI, YOSHINOBU MORIKAWA and YOSHITAKA FUJIWARA†
Faculty of Engineering, Osaka University, Suita, Osaka, Japan

(Received 13 *March* 1984; *in revised form* 30 *July* 1984)

Abstract—A group of solid particles were hung by slender rods in a pipe to make a model of two-phase flow of coarse particles. Pressure gradient and velocities were measured for different types of the models. The drag on the particles (spheres) were obtained from measurements of pressure gradient with some assumptions. The results are summarized as follows. (1) Mean velocities of fluid are lower in the central part of the pipe than in the circumferential part. Turbulence is remarkably increased by particles. The spectrum distribution of turbulent velocity becomes flatter. These results are similar to the gas-solid flow of coarse particles in a vertical pipe. (2) At a large Reynolds number, the drag coefficient per one sphere in the group is larger than that of a single isolated sphere in a uniform flow. When the spheres are arranged along the same line in the longitudinal direction, the drag coefficient becomes smaller as the longitudinal distance between the spheres is shortened.

1. INTRODUCTION

Gas-solid flows are directly related to pneumatic conveying. Many research workers in this field have been putting a priority on investigation of the gross nature of flow such as the relation between the particle flow rate and pressure drop. Though some workers have paid attention to particle motion in the pipe, our understanding of the phenomena inside the pipe is generally poor. Nevertheless, the particle motion is often analysed by applying simple models. For instance, the equations of particle motion is based on the drag law obtained for a single particle in a uniform flow. As the concentration of particles becomes larger, such simple assumptions are not allowed, because mutual interaction between the particles and pipe flow as well as between the particles themselves influences the phenomena. If the Reynolds number based on the particle size and relative velocity is sufficiently low so that the flow can be analysed by using the Stokes approximation, the effects of the mutual interaction are clarified theoretically (Happel & Brenner 1973). However, the Reynolds number common to usual pneumatic conveying is much higher than the one in the region of the Stokes law. Therefore we can not help depending on experimental information with respect to these problems. Lee (1979) and Tsuji *et al.* (1982a) have made experiments on the mutual interaction between two spheres. The flow approaching the spheres was uniform and laminar in their experiments, and thus it is desired that experiments investigating the mutual interaction are made in more realistic situations.

It is difficult to directly measure the fluid drag on a particle in irregular motion in the pipe. Therefore the drag is measured by indirect methods. In one of them, particles are suspended in a vertical pipe flow, and the drag is obtained from measurements of the weight of particles and fluid velocity which keeps the particles in a neutral state of suspension statistically (neither rise nor fall). There are many reports of such experiments in both gas-solid (Harada *et al.* 1964, Siegel 1970, Flatow 1973 and Sunami *et al.* 1978) and liquid-solid flows (Ayukawa *et al.* 1969). It is known that drag coefficients obtained from a suspension experiment take larger values than those of a single particle in the uniform flow. Apart from the suspension experiment, an attempt was also made on estimating the drag coefficient from the pressure gradient along the pipe in which a group of particles exists. Stinzing (1971) hung a group of cylindrical particles in a vertical pipe by using thin threads and measured the pressure gradient. He reported that the drag coefficient per one particle becomes about one-half of the value of the corresponding single particle. This result is

†Present address: Takeda Chemical Industries, Ltd., Yodogawa-ku, Osaka, Japan.

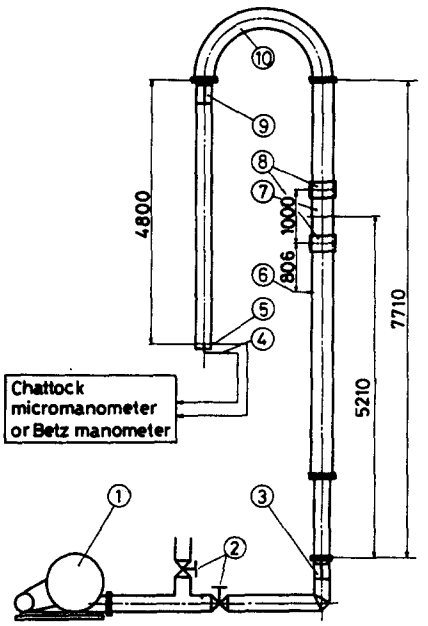

Figure 1. Experimental pipeline. 1 blower, 2 valve, 3 flow straightener, 4 total Pitot tube, 5 pressure tap, 6 reference pressure tap, 7 test section, 8 sleeve, 9 flow straightener, 10 bend.

opposite to the results from the suspension experiment. Brauer (1979) fixed spheres in a square duct and investigated the properties of turbulence by flow visualization.

The present experiment is similar to that of Stinzing (1971), but spherical particles were fixed to a pipe by a number of slender rods which crossed the pipe section in the transverse direction. This paper shows the results of the pressure gradient and drag coefficient as well as distributions of mean and turbulent velocities. From the present work it will be found that fluid drag on particles in pneumatic conveying does not follow the standard drag curve.

2. EXPERIMENTAL ARRANGEMENT

2.1 *Pipeline*

Figure 1 shows the experimental pipeline. The air was supplied from a blower 1 and the flow rate was adjusted by valves 2. The test section was made of a transparent acrylic pipe of

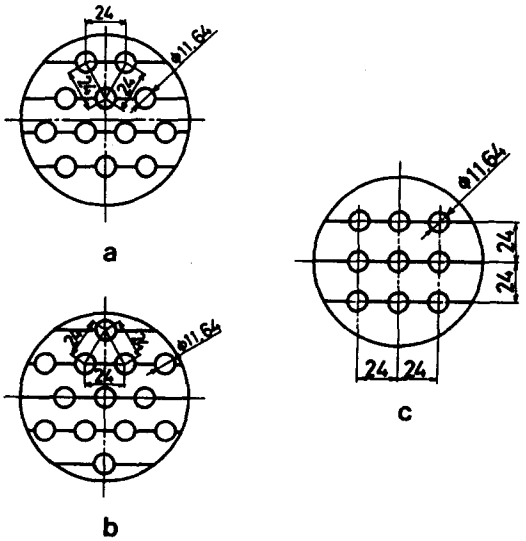

Figure 2. Grid pattern. (a) Hexagonal grid. (b) Hexagonal grid. (c) Square grid and single grid.

No.	Grid	J	I(mm)	$\phi \cdot 10^3$	m	Symbol
1	Hexagonal	46	19.6	6.706	43 ~ 58	
2	Square	26	20	4.731	30 ~ 40	
3	"	21	30	3.154	20 ~ 26	
4	"	21	40	2.366	15 ~ 20	
5	"	15	60	1.577	9.6~13	
6	"	11	80	1.183	7.2~9.6	
7	"	9	100	0.946	5.7~7.6	
8	"	8	120	0.789	4.8~6.4	
9	Single	1				

Table 1. Specifications of models. J, number of grids; l, interval between grids; ϕ, volume concentration of spheres; m, loading ratio

D = 100 mm in diameter and 1000 mm in length, and was situated sufficiently far from the pipe bend. The model of the group of particles was set in the test section. The air flow rate was measured by a Pitot tube at the outlet of the pipeline. The test section had some pressure holes for the measurements of the pressure gradient in the longitudinal direction. Velocities within the pipe were measured by a hot wire probe of I type. The probe was traversed three dimensionally in the x, y and z directions. Preciseness of traverse was about 0.1 mm in all directions.

The analogue signal from the hot wire anemometer was digitized by an A/D converter and processed by a micro computer. The test section was connected to the pipeline by movable sleeves.

2.2 *Model of a group of spheres*

We used plastic spheres of d = 11.6-mm diameter for the model, interconnected by slender metal rods of 0.5 mm in diameter. The following models were used in the present work.

(1) Hexagonal grid model (Model 1)

Spheres were arranged alternately as shown in figure 2(a) and (b), and the distance between two neighboring spheres was 24 mm (=2d). This model had the largest concentration of spheres.

(2) Square grid model (Models 2, 8)

As shown in figure 2(c), square grids having nine spheres at one section are arranged along the pipe. The distance between the grids were varied from 20 to 120 mm. The spheres were lined up in the longitudinal direction.

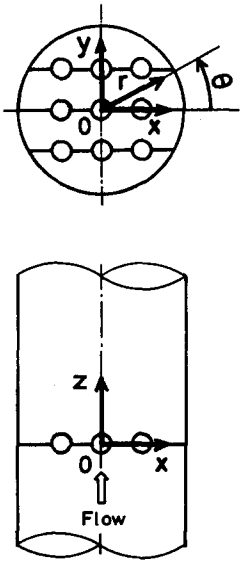

Figure 3. Coordinate system.

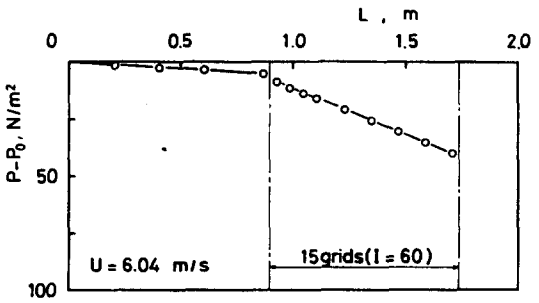

Figure 4. Pressure distribution (model 5).

(3) *Single grid model (Model 9)*

This model corresponds to the case that only one square grid model is set up in the pipe.

Table 1 presents specifications of the models. The loading ratio m in the table corresponds to the case where particles, the density ratio of which to air is 1000, were conveyed at velocities of 0.6 to 0.8 times that of air. The above values of velocity ratio were chosen because velocity ratios in practical pneumatic conveying of coarse particles are usually in such a range. It is seen from the values of m that a particle flow of the Model 1 would correspond to dense phase conveying.

Figure 3 shows the coordinate system used in this paper.

3. RESULTS

3.1 *Pressure gradient*

Figure 4 shows an example of the pressure distribution along the pipe, where L is the distance from the reference point on the upstream side of the model and P is the static pressure. The pressure gradient becomes constant after the first grid. The same tendency was observed in the other models.

Figure 5 presents the pressure distribution of the single grid model, where z is the distance from the grid. The pressure sharply drops just before the point $z = 0$ and shows the minimum value at the position of the grid, which is due to the flow contraction. After the grid, the pressure recovers to some extent and then from the position of $z/d = 12 \sim 13$, it varies with the same gradient as that of the upstream side.

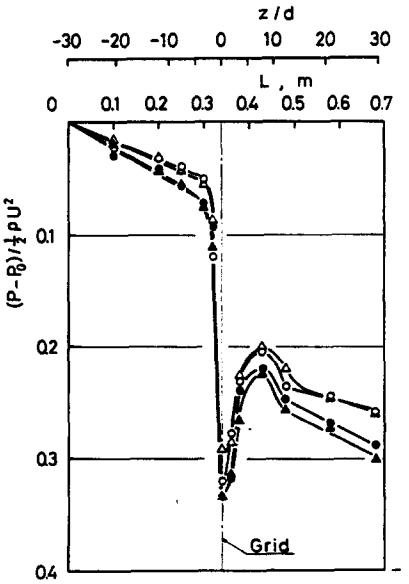

Figure 5. Pressure distribution (single grid model).

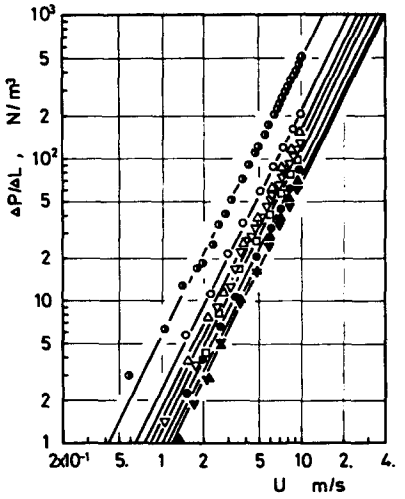

Figure 6. Relation between the pressure gradient and mean velocity relative to the spheres. For legend see Table 1.

Figure 6 shows the relation between the pressure gradient $\Delta P/\Delta L$ and the mean velocity relative to the spheres. This relative velocity U is defined by

$$U = V/(1 - \phi'), \qquad [1]$$

where V is the mean air velocity averaged over the pipe cross section and ϕ' is the volume concentration of the spheres and rods (supports). It is seen in figure 6 that the pressure gradient $\Delta P/\Delta L$ is proportional to U^2 as is the pressure gradient in an ordinary pipe flow.

The total pressure drop consists of the pressure drop due to the friction loss and the one due to the drag force on the spheres and supports. Therefore, the pressure drop ΔP is given as

$$\Delta P = \underset{\text{friction}}{\Delta P_f} + \underset{\text{drag (support)}}{\Delta P_r} + \underset{\text{drag (sphere)}}{\Delta P_s}. \qquad [2]$$

Let us assume the same expressions as the friction loss ΔP_f for the single phase flow and the drag force ΔP_r for the circular cylinder in the uniform flow. Hence,

$$\Delta P_f/\Delta L = (\lambda/D)\, \tfrac{1}{2}\rho U^2, \qquad [3]$$

$$\Delta P_r = C_d\, \tfrac{1}{2}\rho U_r^2\, d_r\, l/(\tfrac{1}{4}\pi D^2). \qquad [4]$$

It is often assumed in analyses of pneumatic conveying that the friction loss obeys the same law as in the single phase flow. Exactly speaking, this assumption is not allowable for the dense phase flow, but in the dense phase flow the friction loss is very small compared with the loss due to drag on particles. Hence, rough estimation of the friction loss does not cause serious errors. Thus the coefficient λ is given by the well-known Blasius formula.

$$\lambda = 0.3164/R_e^{1/4} \quad (R_e = UD/\nu). \qquad [5]$$

Equation (4) is derived from the momentum theorem which gives the relation between the drag force and the pressure drop in the pipe. In (4), l is the total length of the supports and U_r is the velocity relative to the supports. U_r is given by

$$U_r = V/(1 - \psi) = U(1 + \phi')/(1 - \psi) \qquad [6]$$

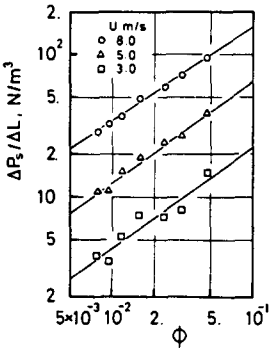

Figure 7. Relation between the pressure gradient and volume concentration of the spheres.

in which ψ is the ratio of the projected area of spheres to the pipe cross section. The drag coefficient C_d is also affected by the fluid turbulence. However, the fraction of ΔP_r is much smaller than that of ΔP_s. Therefore we give C_d as a function of the Reynolds number $U_r d_r/\nu$ following the standard drag curve of the circular cylinder.

Using the expressions of [2] to [6], we obtain the pressure drop caused by the presence of the spheres from the measured values of the total pressure drop. Figure 7 shows the relation between the pressure drop $\Delta P_s/\Delta L$ and the volume concentration of the spheres. From the figure we find that

$$\Delta P_s/\Delta L \propto \phi^{\beta}. \qquad [7]$$

It was also confirmed that the pressure gradient $\Delta P_s/\Delta L$ is proportional to U^2. Therefore, the pressure gradient $\Delta P_s/\Delta L$ is expressed as

$$\Delta P_s/\Delta L = (\zeta/D)\,{}^1\!/_2\rho U^2 \qquad [8]$$

and the coefficient ζ becomes

$$\zeta = \alpha\phi^{\beta}. \qquad [9]$$

Experimental values of α and β obtained by the least square method were

$$\alpha = 2.58, \quad \beta = 0.75. \qquad [10]$$

Summarizing the above results, the total pressure gradient in the pipe having the group of spheres can be given by

$$\frac{\Delta P}{\Delta L} = \left\{\alpha\phi^{\beta} + \lambda + \frac{C_d d_r (l/\Delta L)}{(\pi D/4)}\left(\frac{1+\phi'}{1-\psi}\right)^2\right\}\frac{1}{2}\rho U^2/D. \qquad [11]$$

3.2 *Drag coefficient of sphere*

According to the momentum theorem, the pressure drop is related to the drag on the spheres,

$$\Delta P_s\,{}^1\!/_4\pi D^2 = C_D\,{}^1\!/_2\rho U^2\,{}^1\!/_4\pi d^2 N, \qquad [12]$$

where N is the total number of the spheres in the region concerned. In the case of the single grid model, the pressure distributions in the upper and downstream sides with constant gradients are extrapolated to the position of the grid. The difference in the intercepts

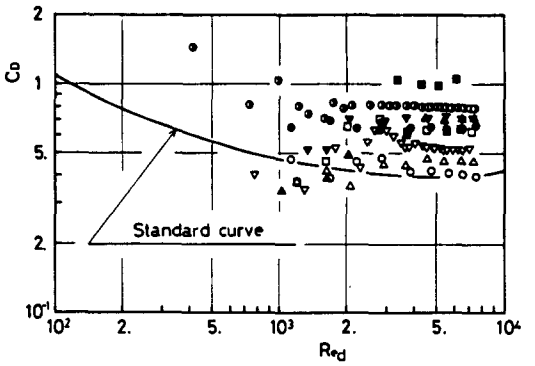

Figure 8. Relation between the drag coefficient and Reynolds number. For legend see Table 1.

between both extrapolated lines gives the pressure drop ($\Delta P_s + \Delta P_r$). Using (4) to subtract ΔP_r from ($\Delta P_s + \Delta P_r$), we obtained the pressure drop ΔP_s and thus C_D for each sphere. The coefficient C_D are plotted against the Reynolds number $R_{ed} = Ud/\nu$ in figure 8, where the standard drag curve (Morsi & Alexander 1972) of a single sphere in the uniform flow is shown for comparison. In general, C_D of the group of spheres take larger values than the standard curve. This is caused by the effects of turbulence and wall as is pointed out by Clift *et al.* (1978). C_D of the square grid models becomes smaller as the concentration becomes larger. The spheres in the square grid models are arranged along the same line in the longitudinal direction, and therefore when the distance between grids is smaller, the rear sphere is located in the wake of the front one, and consequently, the drag force on the rear sphere is reduced.

C_D of the single grid has the largest value among the models, which is because there is no interaction between the grids. The sphere in the hexagonal grid model are arranged alternately along the flow, and thus C_D is large compared with the square grid models even though the distance between the grids is smaller than those square grid models.

The drag coefficient of a sphere in turbulent flow generally depends on the intensity of turbulence and Reynolds number. There is a range of the Reynolds number in which the drag increases markedly due to turbulence (Clift & Gauvin 1978). Stinzing (1971) measured the drag force on a group of cylindrical particles in a similar way to the present method and reported that the drag for one particle in the group is smaller than a single isolated particle. However, it should be noticed that there are several differences between his experiment and ours. First, the pipe flow in his experiment is considered not to be fully developed, and the supports (thin threads) of particles were parallel to the pipe axis. Therefore, the turbulent intensity in his experiment is considered to be small compared with the present case. Consequently, only the effect of particle interaction which reduces the drag was observed, while the effect of turbulence which has the tendency to increase the drag hardly appeared. It is also noted that the Reynolds number and particle size in the experiment of Stinzing (1971) were smaller than the present ones. Even the present results show that C_D becomes smaller than the standard curve for the Reynolds number smaller than 3000. From the above results it is found that the drag on the spheres in a group is affected by the Reynolds number, arrangement of spheres and turbulent intensity.

The present results are the same as the results from an experiment of particle suspension in a vertical flow in that both results indicate that the drag coefficient is larger than the standard curve. However, there are some differences between them as well. In the experiment of particle suspension, the larger the particle concentration, the larger the drag. The square grid models in this experiment show the opposite tendency to that. That is, C_D decreases with increasing the concentration. In actual two-phase flows, particles change relative positions with each other as they move along. Therefore, the square grid model does

not reflect the real condition, but hexagonal or single grid model is near the actual suspension. The drag of spheres in the hexagonal or single grid model is obviously larger than the standard curve. Thus, the drag coefficient larger than the standard curve should be used in an analysis of pneumatic conveying of coarse particles.

Next, the drag coefficient of particles in a fluidized or packed bed is compared with the present one. The drag coefficient corresponding to the Ergun's formula is given as

$$C_D = 200\frac{\phi}{(1-\phi)^2 R_{ed}} + \frac{7}{3(1-\phi)}. \qquad [13]$$

This equation (Soo 1967) shows the effect of the particle concentration on C_D. Substituting the present value of ϕ to [13] and comparing C_D with the present results, it is found that C_D calculated from [13] becomes several times larger than the largest value in the present experiment. The range of ϕ in the fluidized or packed bed is much larger than those in the present experiment. Therefore it is no wonder that the empirical formula for large ϕ can not be applied to the case for small ϕ.

3.3 *Velocity distribution*

Figure 9 shows contour lines of equal mean velocity and turbulent intensity. In this paper, the turbulent intensity is defined by

$$T_u = \sqrt{(u'^2)^{1/2}}/\bar{u} \qquad [14]$$

in which u' and $\bar{u}$ are, respectively, the longitudinal components of fluctuating and time-averaged mean velocities. The figures show characteristic structures of flow field corresponding to the position of spheres. That is, the mean velocity is small and turbulent intensity is large behind the sphere.

Figure 10 shows the distributions of mean velocity and turbulent intensity. The mean velocity distributions differ markedly from that of the single phase pipe flow even at the most downstream section. Also, a tendency is observed that the radial position of the maximum velocity approaches to the wall as the flow moves downstream. The distribution along the line $\theta = 45°$ shows the same tendency as in figure 10 in spite that the sphere exists near the wall on the line $\theta = 45°$. Measurements of some gas-solid pipe flows show that the mean velocity distributions are concave with the center velocity being lower than circumferential velocity (Vollheim 1965 and Tsuji *et al.* 1982b, 1984). The present distribution shown in figure 10 is qualitatively the same as such results.

The distribution of turbulent intensity changes from an uneven profile to a flat one as the flow moves downstream, but quantitatively the intensity remains higher compared to

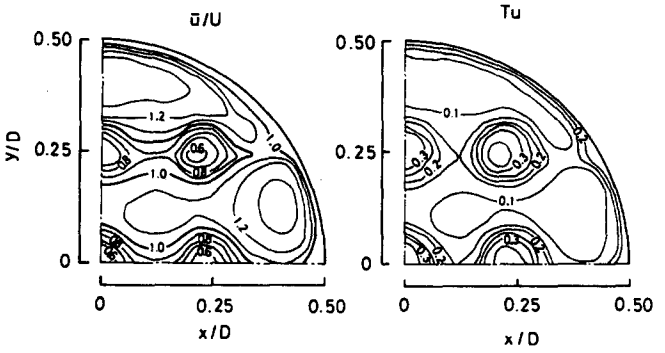

Figure 9. Contour lines of equal mean velocity and turbulent intensity. (Model 5, $z/d = 2$, $U = 5.25$ *m/s*.)

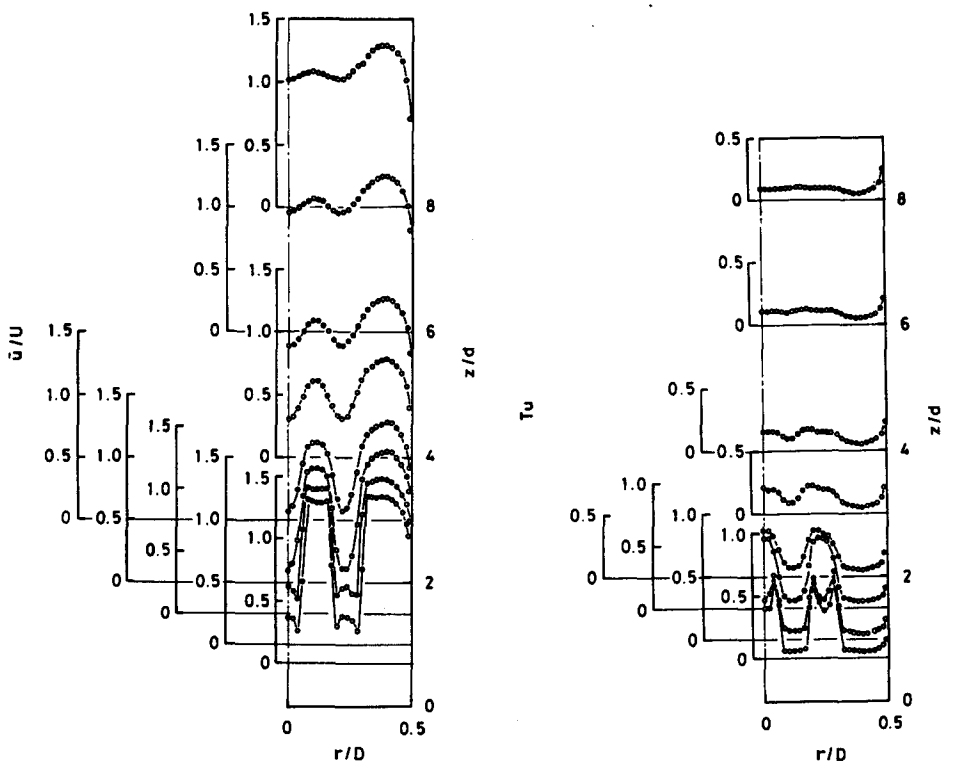

Figure 10. Distributions of mean velocity and turbulent intensity. (Model 8, $\theta = 90°$, $U = 5.21$ m/s.) (a) Mean velocity. (b) Turbulent intensity.

ordinary pipe flows. For instance, the intensity at the pipe center is three times larger than that of the ordinary pipe flow even at the most downstream section $z/d = 8$. Recent measurements by Laser Doppler velocimeters show that the turbulent intensities increase in the presence of large particles (Tsuji *et al.* 1982, 1984), which qualitatively agrees with the above results.

We measured the distributions of mean and turbulent velocities along the line $\theta = 45°$ as well as $\theta = 90°$ in order to see the effects of the supports. It was found that the effects were not observed in the downstream section from $z/d = 3$. Measurements of the flow fields were not made in the case of the hexagonal grid model because of difficulties of traversing the hot wire probe.

In this work we paid attention to the probability density function of the fluctuating velocities, because it is also an important property of fluctuation. The characteristic features

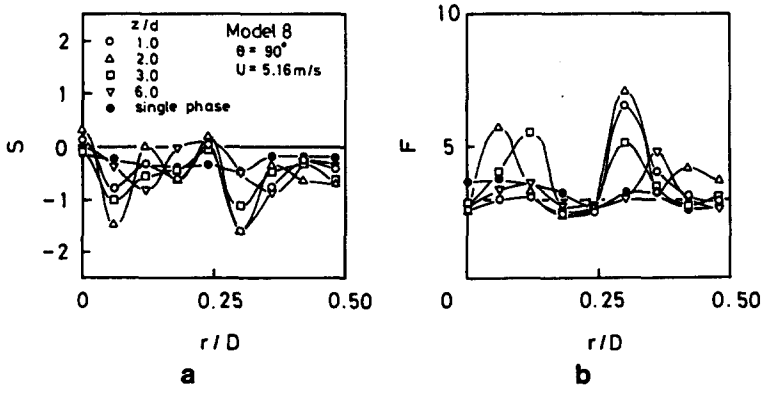

Figure 11. Skewness and flatness factors. (a) Skewness factor. (b) Flatness factor. [For legend see (a).]

of the function are generally seen in the skewness and flatness factors which are defined by

$$S = \overline{u'^3}/(\overline{u'^2})^{3/2},$$
$$F = \overline{u'^4}/(\overline{u'^2})^2. \qquad [15]$$

The results of S and F are shown in figure 11 instead of their distributions. The normal distribution of the probability gives 0 and 3, respectively, to S and F. The skewness and flatness factors in the wake region of spheres largely differ from those values of the normal distribution, i.e. S is negative and F is larger than 3. The same tendency in S and F as the above results were also observed in measurements of the gas-solid pipe flow (Tsuji *et al.* 1982).

Figure 12 shows the magnitude spectra of the turbulent velocities which are obtained by an FFT (fast Fourier transform) analyser. The magnitude spectrum is defined by

$$\overline{u'^2} = \int_0^\infty S_M^2(f)\,df. \qquad [16]$$

The results in other sections were similar to figure 12. We find that the spectrum in the presence of spheres is flat compared with the one of the sphere-free flow. Such a flattening effect of the sphere is observed also in the spectrum of a duct flow with fixed spheres, as Brauer (1979) reviewed. Characteristic properties of the wake of spheres clearly appear in the mean and turbulent velocity distributions, and so we expected that there would be a peak in the spectrum distribution which corresponds to shedding vortices from the spheres. Contrary to our expectation, such a peak was scarcely found in most measuring points. However, at some points, a weak peak was found which is indicated by an arrow in figure 12. The Strouhal numbers corresponding to the peak were scattered from $S_t = 0.10$ to 0.23.

Acknowledgement—The authors wish to thank Mr. T. Funabiki and Mr. A. Sato for their assistance in the present experimental work.

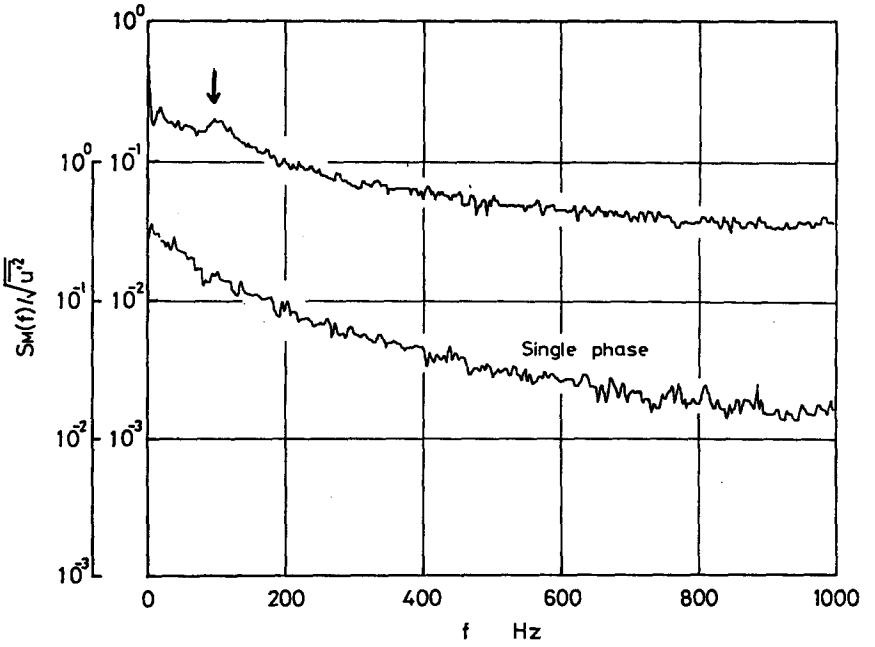

Figure 12. Spectra of fluctuating velocities (model 8, $\theta = 90°$, $r/D = 0.12$, $z/d = 3$, $U = 5.16$ *m/s*).

NOMENCLATURE

C_D drag coefficient of sphere
C_d drag coefficient of cylinder
D pipe diameter
d diameter of sphere
d_r diameter of rod (support)
F flatness factor defined by [15]
I interval between grids
J number of grids
L longitudinal distance from the reference point
l length of rods
m loading ratio
N number of spheres
P static pressure
ΔP pressure drop
ΔP_f pressure drop due to friction loss
ΔP_r pressure drop due to drag on rods
ΔP_s pressure drop due to drag on spheres
R_e Reynolds number UD/ν
R_{ed} Reynolds number Ud/ν
r radius
S skewness factor defined by [15]
S_M amplitude spectrum defined by [16]
T_u turbulent intensity
U velocity defined by [1]
$\bar{u}$ local mean velocity
u' turbulent velocity
V superficial velocity based on unobstructed flow area
x, y, z coordinates shown in figure 3
θ angle shown in figure 3
λ friction coefficient
ϕ volume concentration of spheres
ϕ' volume concentration of spheres and rods
ψ ratio of the projected area of spheres to the pipe cross section

REFERENCES

AYUKAWA, K., OCHI, J. & SINMYO, S. 1970 The effects of wall and concentration on the terminal velocities of solid particles. *Bull. JSME* **13-62**, 996–1004.

BRAUER, H. 1979 Turbulenz in mehrphasigen Strömungen. *Chem. Ing. Tech.* **51**, 934–948.

CLIFT, R. & GAUVIN, W. H. 1971 Motion of entrained particles in gas streams. *Can. J. Chem. Eng.* **49**, 439–448.

CLIFT, R., GRACE, J. R. & WEBER, M. E. 1978 *Bubbles, drops and particles.* Academic Press, New York, pp. 226 and 266.

FLATOW, J. 1973 Untersuchungen über die pneumatische Flugförderung in lotrechten Rohrleitungen. *VDI Forsch. Heft.* 555.

HAPPEL, J. & BRENNER, H. 1973 *Low Reynolds number hydrodynamics.* Noordhoff International.

HARADA, S. NARUI, H., SHIMADA, K. & FUKUSHIMA, T. 1964 Fundamental research on pneumatic conveying. *Trans. Jpn Soc. Mech. Engrs.* **30-210**, 231–235.

LEE, K. C. 1979 Aerodynamic interaction between two spheres at Reynolds numbers around 10^4. *Aeronaut. Q.* **30**, 371–385.

MORSI, S. A. & ALEXANDER, A. J. 1972 An investigation of particle trajectories in two-phase flow systems. *J. Fluid Mech.* **55,** 193–208.

SIEGEL, W. 1970 Experimentelle Untersuchungen zur pneumatischen Förderung körniger Stoffe in waagerechten Rohren und Überprüfung der Ähnlichkeitsgesetze. *VDI Forsch. Heft.* 538.

SOO, S. L. 1967 *Fluid dynamics of multiphase systems.* Blaisdell Publishing, pp. 185–189.

STINZING, H. D. 1971 Fluid drag on clouds consisting of solid particles enclosed in a pipe. Proc. 1st. Int. Conf. on Pneumatic Transport of Solids in Pipes, Paper C6, BHRA *Fluid Engng.*, Cranfield, U.K.

SUNAMI, T., MORIYA, S., TANAKA, S. & MORIKAWA, Y. 1978 A study of airlift for the feeder of solids. *Bull. JSME* **21-153,** 447–454.

TSUJI, Y., MORIKAWA, Y. & TERASHIMA, K. 1982a Fluid-dynamic interaction between two spheres. *Int. J. Multiphase Flow* **8-1,** 71–82.

TSUJI, Y. & MORIKAWA, Y. 1982b LDV measurements of an air-solid two-phase flow in a horizontal pipe. *J. Fluid Mech.* **120,** 485–409.

TSUJI, Y., MORIKAWA, Y. & SHIOMI, H. 1984 LDV measurements of an air-solid two-phase flow in a vertical pipe. *J. Fluid Mech.* **139,** 417–434.

VOLLHEIM, R. 1965 Die Förderung von Festkörper-Luft-Gemischen in Rohren. *Maschinenbautechn.* **14-9,** 455–460.